Revision 2

UHP Ti-chondrodite in the Zermatt-Saas serpentinite: constraints on a new tectonic scenario

Pietro Luoni[1], Gisella Rebay[2], Maria Iole Spalla[1] and Davide Zanoni[1]

[1]Università degli Studi di Milano, Dipartimento di Scienze della Terra 'A. Desio', Via Mangiagalli, 34 - 20133 Milano, Italy

[2]Università degli Studi di Pavia, Dipartimento di Scienze della Terra e dell'Ambiente, Via Ferrata, 1 - 27100 Pavia, Italy

pietro.luoni@unimi.it , gisella.rebay@unipv.it , iole.spalla@unimi.it , davide.zanoni@unimi.it

ABSTRACT

We focus on the key role of different Ti-humite minerals in subducted serpentinites as possible indicators of extreme pressure conditions. The occurrence of Ti-chondrodite and/or Ti-clinohumite assemblages in the eclogitized serpentinites of the Zermatt-Saas Zone (ZSZ) of the Western Alps allows the recrystallization of such rocks at UHP conditions (P= 2.8-3.5 GPa, T= 600-670 °C) to be determined. Such conditions are similar to those registered by the nearby Cignana unit, a main Alpine area for UHP metamorphism, where coesite and microdiamond have been found. In ZSZ serpentinites, the new UHP assemblage predates the previously-recognised HP-UHP paragenesis, which was recently dated at 65 Ma. This finding opens up a new interpretation for the petrologically and structurally well-constrained HP/UHP records, especially because all other ages for HP-UHP metamorphism in the ZSZ are much younger, and for the size of UHP units. Our findings suggest that ophiolites in the axial zone of collisional belts are a mosaic of oceanic lithosphere slices that recorded contrasted thermal and mechanical evolutions during their physical trajectories in the subduction wedge.

KEYWORDS: Ti-clinohumite & Ti-chondrodite assemblages, integrated mineralogical and structural analysis, Alpine subduction, Western Alps.

INTRODUCTION AND GEOLOGICAL SETTING

HP–UHP mineral assemblages are the trademark of subduction zones. The most widely known are metamorphic coesite and diamond inclusions in host grains in eclogite-facies crust of the Western Alps, Norway, Central Europe, China and Kazakhstan, and majoritic garnet and Si-bearing spinel in garnet peridotite (e.g., Ernst and Liou 2008; Frezzotti et al. 2011). Recognized as upper mantle minerals from Colorado Plateau kimberlites (Aoki et al. 1976; Smith et al. 1977), Ti-clinohumite and Ti-chondrodite, are also part of HP-UHP assemblages in ultramafites from China and the Western Alps (Scambelluri and Rampone 1999; Shen et al. 2015). Shen et al. (2015) proposed conditions of 2.7 GPa and 550–660 °C for the assemblage Ti-chondrodite (Ti-Chn) + Ti-clinohumite (Ti-Chu) + Atg + Chl + Ol + Spl, demonstrating that Ti-Chn + Ti-Chu assemblages are indicators of UHP conditions in serpentinized Ti-rich ultramafites (mineral abbreviations after Whitney and Evans, 2010). The experimental demonstration of Ti-humite minerals defining HP–UHP conditions encouraged us to examine in detail fabrics and mineral assemblages in Valtournanche (Rebay et al. 2012), in order to determine the microstructural relationships of Ti-Chu and/or Ti-Chn relics with the dominant HP/UHP foliation (S2) in these rocks. The occurrence of UHP rocks in the axial zones of orogenic belts has fuelled debates on geodynamic environment (i.e. subduction, collision, late orogenic extension), exhumation mechanisms, and the timing of exhumation, which strongly influence the preservation of UHP assemblages (Ernst and Liou 2008). In the Alps, findings of UHP phases have led to identification of hectometer to kilometer UHP tectonic units within HP nappes. Coesite relics (Reinecke 1991, 1998) and microdiamond (Frezzotti et al. 2011) occur in the Cignana Lake Unit (CLU) at the tectonic contact between the Zermatt-Saas Zone (ZSZ) and the Combin Zone (CZ). The shape, size, and exhumation environment of these UHP tectonic units are discussed. The occurrence of Ti-humites makes serpentinites a new key target for identification of UHP units.

The ZSZ (Fig. 1a, b) was derived from the internal portion of the Piedmont oceanic realm. It was trapped in the suture zone of the Western Alps during Alpine convergence (e.g Spalla et al. 2010). It comprises serpentinite, meta-gabbro, meta-rodingite, meta-basalts and various meta-sediments. The metamorphism of the ZSZ is typical for eclogite facies conditions, locally overprinted by greenschist-facies mineral assemblages (commonly interpreted as exhumation-related). Peak P–T estimates range from 1.9–2.2 GPa and 500–600 °C to 2.3–2.8 GPa and 580–660 °C in different portions of the ZSZ (Bucher et al. 2005; Martin et al. 2008; Bucher and Grapes 2009; Zanoni et al. 2016). Such a wide P–T span suggests that different portions of the ZSZ underwent different tectono-metamorphic evolutions. In contrast, a common, and consequently uniform, evolution of the entire ZSZ was proposed by Angiboust and Agard (2010), with metamorphism peaking at 2.3 ± 0.1 GPa and 540 ± 40°C. UHP conditions of 2.7 – >3.2 GPa and 590–630 °C have been recorded in small slices of oceanic rocks at the boundary between the ZSZ and CZ, at Lago di Cignana (Fig. 1c) (Groppo et al. 2009 and refs. therein). Protholith U/Pb ages range from 153–164 Ma (metabasites; Rubatto et al. 1998) to 162–168 Ma (serpentinites; Rebay et al. 2018). Peak metamorphic ages are 71–38 Ma so that subduction might have been active already at 80 Ma (Table 1 in Rebay et al. 2018), indicating a wide time interval of re-equilibration during subduction, and supporting a heterogeneous evolution of ZSZ. In particular, the dominant HP/UHP foliation (S2) of upper Valtournanche has been dated at 65.5 ± 5.6 Ma (Rebay et al., 2018).

MESOSTRUCTURE AND ROCK TYPES

In ZSZ serpentinites from upper Valtournanche, continuous structural mapping of superposed fabric elements allows the recognition of four groups of ductile structures, where D1–D3 are synmetamorphic, and D4 consists of open folds and local disjunctive cleavage (Rebay et al. 2012; Zanoni et al. 2012, 2016). South of Cervinia (Fig. 1b), serpentinites contain Mag-rich layers alternating with dm-thick Cpx- and Ol-rich layers and lenses, Ti-Chu and Ol veins (Fig. 1d), and rare rodingite dykes. Here, coherently with observations at the regional scale, the S2 composite foliation is the dominant fabric in serpentinites, wrapping cm-sized oval Cpx porphyroclasts, and transposing Ol veins. S2 intersects Mag-, Cpx-, and Ol-rich layers that are locally rimmed by Ti-Chu aggregates. Different pre-D2 relics are preserved: a foliation in the cm-sized D2 lithons; humite-bearing veins marking cm-sized tight fold hinges or disrupted into lenticular aggregates mantled by S2; mm- to cm-thick Mag-rich and up to 10 cm-thick Ol-rich layers (Fig. 1e) marking relic folded foliation. These relics are scattered and their dispersion inhibits any walking-correlation between them. For this reason, they will be hereafter labeled as pre-D2 (see also Supplementary 1).

MICROSTRUCTURES AND PARAGENESES

The S2 foliation in serpentinite is marked by shape preferred orientation (SPO) of Ti-Chu2 + Atg2 ± Ol2 + Chl2 + Mag2 ± Cpx2 (numbers denote the relative age of associated fabrics; Rebay et al. 2012, 2018) and intersects or wraps around pre-D2 humite-bearing veins and lenses in which Ti-Chn ± Ti-Chu occur. Pre-D2 relics are Mag, Ti-Chn, Ol or Cpx porphyroclasts, and veins or lenticular micro-aggregates containing Ti-Chn, Ti-Chu, Ol, and Spl (currently not preserved (ex-Spl) and replaced by Ilm with Mag exsolutions), variably transposed and recrystallized during S2 development. Cpx and Cr-rich Ol porphyroclasts, wrapped by S2 and containing exsolutions of Ti-humites, are pre-subduction mantle or ocean floor relics (e.g. Zanoni et al. 2012). Lenses of Ti-Chu + Ol polygonal aggregates are elongated parallel to S2.

Well-preserved pre-D2 Alpine fabrics and Ti-rich assemblages have been found in serpentinite and in veins. Within the veins, red-orange twinned Ti-Chn porphyroclasts, reaching 4 mm (Fig. 1f), enclose randomly oriented Atg and Ilm with lobate grain boundaries, which can be interpreted as relics. Ti-Chn porphyroclasts are cut by fractures filled by Atg2 + Ti-Chu2 and rimmed by polygonal Ti-Chu. Twins are simple or tapering lamellae. In the veins, porphyroclasts of Spl ± Ti-Chn, are rimmed by aggregates of small, equigranular polygonal Ti-Chn + Ti-Chu + Ilm + Mag, forming a core-mantle structure. Ol-porphyroclasts (up to 5 mm) with tapering Ti-Chu exsolution lamellae show rims with Atg and Ti-Chu inclusions. The veins are variably transposed by S2 (Ti-Chu2 + Ol2 + Atg2 + Mag2 + Chl2).

In serpentinite, scattered pre-D2 Mag porphyroclasts, up to 5 mm and wrapped by S2, are locally zoned, preserve Cr-rich cores, and are cut by pre-D2 fractures filled by Ti-Chn + Atg + Mag. Polygonal Ol2 + Ti-Chu2 occur in pressure shadows of Ol porphyroclasts and show SPO gradually parallelized into S2. Moreover, lenticular micro-aggregates of Ti-Chu + Ilm ± Ti-Chn with minor Atg and Chl, with SPO parallel to S2, replace Ti-Chn porphyroclasts. Ti-Chn occurs in elongated crystals kinked by D2. Pre-D2 Cpx porphyroclasts, with lamellae of Ilm + Mag + Chl + Ti-Chu or Ti-Chn, reach 15 mm and are deformed and kinked. Rarely, they preserve inclusion-free augitic cores. Cpx has Cpx2 rims or pressure shadows of Cpx2 + Atg2 + Chl2. The pre-D2 Cpx grains are cut, at high angle with S2, by conjugate veins of Ti-Chu (polygonal aggregates in Fig. 1g). In Ol-rich layers, S2 (Atg2 + Ol2 + Mag2) wraps pre-D2 Ol and Cr-magnetite porphyroclasts (<5 mm). Ol porphyroclasts, with Cpx, Atg and Mag inclusions, are locally rimmed by a corona and have pressure shadows of polygonal Ol + Atg + Mag.

In summary, the microstructural relationships (see also Supplementary 1) demonstrate the following sequence of assemblages and fabrics:

1) a pre-D2 mineral assemblage consisting of Cpx or Ol + Ti-Chn + Spl porphyroclasts + Atg ± Chl; the rare relics of Ol, Cpx, and Cr-rich Mag porphyroclasts are yet earlier, and we interpret them as pre-Alpine minerals (López Sánchez-Vizcaíno et al. 2009 and refs. therein; Zanoni et al. 2012, 2016).

2) Ti-Chn + Ti-Chu polygonal aggregates (with minor Chl + Ilm + Mag + Atg + Cpx or Ol) can be interpreted as either predating S2 or being synkinematic with the early stages of S2 development (hereafter, pre-D2 to early D2).

DOI: https://doi.org/10.2138/am-2018-6460

3) D2 mylonitic assemblage is Ti-Chu2 + Atg2 + Chl2 + Mag2 ± Ol2 ± Cpx2.

A similar sequence of fabrics has been observed in olivine-rich layers. With respect to experimental data, this sequence of successive assemblages indicates that the transition from pre-D2 to D2 reflects the transition from UHP to HP conditions (Figs 15 and 17 in Shen et al. 2015).

MINERAL COMPOSITIONS & METAMORPHIC CONDITIONS

Minerals were analyzed with a JEOL 8200 Super Probe (WDS), at 15 kV accelerating voltage and a beam current of 15 nA. Natural silicates were used as standards and matrix corrections were calculated using the ZAF procedure. Ti-Chn and Ti-Chu were recalculated on the basis of 13 and 7 cations, respectively. Ol trace elements were obtained, from inclusion-free crystals (from SEM images), at Pavia CNR-IGG with a LA–ICP–MS system coupling a 266 nm Nd: YAG laser probe with a double focusing magnetic-sector mass spectrometer, using NIST 610, NIST 611 and BCR2 standards, and GLITTER data processing (Tiepolo et al. 2003). Spot size was 40-55 µm, laser frequency 10Hz, acquisition was for 40-60 seconds preceded and followed by at least 40 seconds background counting (see Table 1 and Supplementary 1 file).

Ti-Chn has 0.32–0.41 Ti apfu and M/Si (M= Mg+Fe+Mn+Ni+Ti) of 2.43–2.62. Polygonal aggregates have higher M/Si and Ti than porphyroclasts (Fig. 2a): for one sample in the range reported by González-Jiménez et al. (2017), whereas others have consistently higher M/Si probably due to bulk composition. X_{Mg} (Mg/(Mg+Fe)) is 0.88–0.92. Mn is <0.04 apfu. *Ti-Chu* composition varies slightly with microstructural position: Ti-Chu in polygonal aggregates has lower M/Si and Mg+Fe+Ti+Ni than Ti-Chu2; Ti is 0.32 – 0.39 apfu, but usually lower in polygonal aggregates (Fig. 2a). The Ti-Chu exsolutions in pre-D2 Ol have lower Ti content than Ti-Chu2; similarly, X_{Mg} is higher in polygonal Ti-Chu aggregates than in Ti-Chu2. Mn is <0.05 apfu and X_{Mg} 0.89–0.95. In serpentinites, *Ol* in veins is the richest in Mg (X_{Mg} 0.90–0.96); Ol associated with Ti-Chn porphyroclasts is the richest in Fe (X_{Mg}

0.90–0.91). In Ol porphyroclasts within Ol-rich layers X_{Mg} is 0.89–0.96; in polygonal Ol, X_{Mg} has a similar range. Mn is <0.02 apfu. In Ti-Chn + Ti-Chu veins, *Atg* shows the widest variation in Al, Si, Mg, and Fe content. Pre-D2 Atg is generally Mg, Fe, and Al poor, whereas Atg2 is richer in Si. *Chl* is always penninite. In serpentinites, *Mag* in polygonal aggregates and Mag2 have small amounts of Cr; locally Mag2 is pure magnetite. Pre-D2 Mag porphyroclasts have chromite-rich cores (Mg-chromite + chromite <40%). The cores of pre-D2 *Cpx* porphyroclasts are augite; Cpx2 has Al <0.6 apfu, higher than the diopsidic rims around the porphyroclasts.

In Ol-rich layers, Ol has variable Cr and Al contents (acquired for T-estimation, e.g. De Hoog et al. 2010, all reported values are above detection limits): 2.43–17.90 and 0.33–3.59 ppm in Ol porphyroclasts, and 2.06–5.98 and 0.88–2.05 ppm in polygonal Ol, respectively. Ol with Cr >10 ppm is interpreted as pre-Alpine relic.

Pre-D2 P–T conditions (Fig. 2b) are inferred using a combination of methods. Experimental results in Ti-rich bulks (Shen et al. 2015) limit Ti-Chn + Ti-Chu stability field at minimum P-values of 2.6–3.1 GPa at 560–700 °C by the univariant Ti-Chn out (field above the Ti-Chn out in Fig. 2b), which would constrain P_{min} for the pre-D2 assemblage Ti-Chn + Ol + Spl + Chl + Atg. Higher Ti contents enlarge the Chn stability field towards lower P and therefore the occurrence of Ti-rich phases (e.g. relic Ilm, Ilm after Spl) in our rocks suggest to refer to the Schreinemaker P-T grid proposed by Shen et al. (2015) to estimate more reliable P conditions for pre-D2 to early D2 (Reactions 1 and 2, fig. 2b). To this purpose, T conditions shall be constrained. In serpentinite, temperatures for the pre-D2 to early D2 polygonal assemblages were calculated with THERMOCALC (Powell et al. 1998) using the Average T method (AvT): Ol or Cpx (Fo-Fa/Di-Hed), Chl (Clin-Daph), Mag (Mt, Usp), Ilm (Ilm-Geik) solid solutions (calculated using Ax program, end-members names as in Ax instructions) were used with Atg and Chu (with no Ti) end-members. Since Fe-Mg exchange is poorly constrained, the obtained values, of 640 ± 70 °C (2σ), calculated between 2.1 and 3.0 GPa, are affected by high errors. In Ol-rich layers, the Al content of Ol (De Hoog et al. 2010) indicates 645 ± 55 °C for pre-D2 (calculated from 2.7-3.5 GPa) (Ol porphyroclasts), and 635 ± 45 °C for pre-D2 to early D2 (calculated from 2.0-3.0 GPa) (Ol-polygonal aggregates), (Fig. 2b). The Atg-out curve indicates T < 670 °C for Opx-free assemblages. The stability of Atg varies as a function of bulk composition towards lower T in Ti-free systems (<640-650 °C Rebay et al. 2012; Padrón-Navarta et al. 2013), but we refer to the T values estimated for Ti-rich systems by Shen et al. (2015), which have more similar composition to the studied rocks. Considering the sequence of the inferred assemblages, i.e. 1) pre-D2 with Ti-Chn (without Ti-Chu and with Spl), 2) pre-D2 to early D2 with Ti-Chu + Ti-Chn and 3) synD2 with Ti-Chu, we propose for the estimated T interval, a P_{min} of 2.8-3.0 GPa and a P_{max} of 3.5 GPa for pre-D2 assemblage 1. Assemblage 2 (pre-D2 to early D2) is stable at similar T-interval (570 to 670°C), for which the coexistence of Ti-Chu and Ti-Chn indicates a P range from 2.1 to 3.0 GPa (see Fig. 2b, reaction 1). Finally, the syn-S2 paragenesis (without Ti-Chn) is stable below the Ti-Chn out reactions in all compositions, at P–T conditions similar to those previously determined for syn-D2 in serpentinite and rodingite (Rebay et al. 2012; Zanoni et al. 2016).

DISCUSSION & IMPLICATIONS

The different chronologically- and petrologically-framed types of Ti-humites allows UHP conditions in serpentinites to be identified, in rocks generally not considered to be diagnostic from a pressure point of view. The diagnostic UHP assemblage (Ti-Chn + Atg + Chl + Spl + Ol /Cpx) predated the dominant 65 ± 5.6 Ma old foliation (S2 in Rebay et al., 2018) that formed at the limit between HP and UHP and up to now was considered to be at the metamorphic climax conditions. The peak-conditions recorded in the ZSZ serpentinites are therefore increased to 2.8–3.5 GPa and 600 – 670 °C. The rocks were successively re-equilibrated at 2.1–3.0 GPa and 570-670 °C during pre-D2 to early D2. Finally, the rocks were re-equilibrated at 2.2–2.8 GPa and 580–660 °C during S2 development (Rebay et al. 2012; Zanoni et al. 2016). Consequently, the age of the new P-peak needs to be earlier than the Paleogene-

Cretaceous boundary. The implications of this finding are significant (i) for Alpine geology and, more in general, (ii) for the interpretation of burial and exhumation processes of UHP/HP meta-ophiolites in collisional belts.

In the framework of the Alpine belt, these rocks, together with others preserving UHP assemblages, are distributed along the tectonic contact between ZSZ and CZ and record different and diachronic peak pressures. For example, the nearby LCU underwent UHP (600 °C and P > 3.2 GPa) at 42 ± 2 Ma (see Rebay et al. 2018, table 1 for refs), much earlier than the rocks studied in this paper. Consequently, the P-climax was recorded at different depths and times in different portions of ZSZ, which therefore consists of a mosaic of tectonometamorphic units probably accreted at depth. Possibly only a few vestiges of these units preserving UHP signatures survived the main regional foliation development. Others may still be detected.

From a more general point of view, the resulting tectonic framework of this key area for the eclogitized oceanic crust, points out that ophiolites in the axial zone of collisional belts correspond to a mosaic of slices of oceanic lithosphere recording different thermal and structural evolutions during their burial and exhumation trajectories in the mantle wedge of a subduction system.

ACKNOWLEDGMENTS: reviewers J.-M. Lardeaux, J.A. Padrón-Navarta, J. Hermann and editor I. Swainson provided advice greatly improving the paper. Funding by PSR2015-1716DZANO_M and Studio Ciocca. We thank A. Langone (IGG-CNR Pavia) for his assistance with LA-ICP-MS.

REFERENCES

Angiboust, S., and Agard, P. (2010) Initial water budget: The key to detaching large volumes of eclogitized oceanic crust along the subduction channel? Lithos, 120, 453–474.

Aoki, K. I., Fujino, K., and Akaogi, M. (1976) Titanochondrodite and titanoclinohumite derived from the upper mantle in the Buell Park kimberlite, Arizona, USA. Contributions to Mineralogy and

DOI: https://doi.org/10.2138/am-2018-6460

Petrology, 56, 243-253.

Bucher, K., and Grapes, R. (2009) The eclogite-facies Allalin gabbro of the Zermatt-Saas ophiolite, Western alps: A record of subduction zone hydration. Journal of Petrology, 50, 1405–1442.

Bucher, K., Fazis, Y., de Capitani, C., and Grapes, R. (2005) Blueschists, eclogites, and decompression assemblages of the Zermatt-Saas ophiolite: High-pressure metamorphism of subducted Tethys lithosphere. American Mineralogist, 90, 821–835.

De Hoog, J.C.M., Gall, L., and Cornell, D.H. (2010) Trace-element geochemistry of mantle olivine and application to mantle petrogenesis and geothermobarometry. Chemical Geology, 270, 196–215.

Ernst, W.G., and Liou, J.G. (2008) High- and ultrahigh-pressure metamorphism: Past results and future prospects. American Mineralogist, 93, 1771–1786.

Forster, M., Lister, G.S., Compagnoni, R., Giles, R., and Hills, D. (2004) Mapping of oceanic crust with“ HP” to“ UHP” metamorphism: The Lago di Cignana Unit, (Western Alps). Mapping geology in Italy. 279-286. APAT - Servizio Geologico d'Italia, Roma 2004, Map 33, S.EL.CA. Firenze.

Frezzotti, M.L., Selverstone, J., Sharp, Z.D., and Compagnoni, R. (2011) Carbonate dissolution during subduction revealed by diamond-bearing rocks from the Alps. Nature Geoscience, 4, 703–706.

González-Jiménez, J. M., Plissart, G., Leonardo, N. G., Padrón-Navarta, J. A., Aiglsperger, T., Romero, R., Marchesi, C., Moreno-Abril, A. J., Reich, M. Barra, F. and Morata, D. (2017). Ti-clinohumite and Ti-chondrodite in antigorite serpentinites from Central Chile: evidence for deep and cold subduction. European Journal of Mineralogy. Prepubblication article.

Groppo, C., Beltrando, M., and Compagnoni, R. (2009) The P-T path of the ultra-high pressure Lago Di Cignana and adjoining high-pressure meta-ophiolitic units: Insights into the evolution of the subducting Tethyan slab. Journal of Metamorphic Geology, 27, 207–231.

López Sánchez-Vizcaíno, V., Gómez-Pugnaire, M.T., Garrido, C.J., Padrón-Navarta, J.A., Mellini, M., (2009). Breakdown mechanisms of titanclinohumite in antigorite serpentinite (Cerro del Almirez massif, S. Spain): A petrological and TEM study. Lithos, 107, 216–226.

Martin, S., Rebay, G., Kienast, J.R., and Mevel, C. (2008) An eclogitic oceanic palaeo-hydrothermal field from the St. Marcel Valley. Ofioliti, 1, 49–63.

Powell, R., Holland, T.J.B., and Worley, B. (1998) Calculating phase diagrams involving solid solutions via non-linear equations, with examples using THERMOCALC. Journal of Metamorphic Geology, 16, 577–588.

Padrón-Navarta, J.A., López Sánchez-Vizcaíno, V., Hermann, J., Connolly, J.A.D., Garrido, C.J., Gómez-Pugnaire, M.T. and Marchesi, C. (2013) Tschermak's substitution in antigorite and consequences for phase relations and water liberation in high-grade serpentinites. Lithos, 15, 186–196.

Rebay, G., Spalla, M.I., and Zanoni, D. (2012) Interaction of deformation and metamorphism during subduction and exhumation of hydrated oceanic mantle: Insights from the Western Alps. Journal of Metamorphic Geology, 30, 687–702.

Rebay, G., Zanoni, D., Langone, A., Luoni, P., Tiepolo, M., and Spalla, M.I. (2018) Dating of ultramafic rocks from the Western Alps ophiolites discloses Late Cretaceous subduction ages in the Zermatt-Saas Zone. Geological Magazine, 155, 298–315.

Reinecke, T. (1991) Very high pressure metamorphism and uplift of coesite-bearing metasediments from the Zermatt-Saas Zone, Western Alps. European Journal of Mineralogy, 10, 7–17.

Reinecke, T. (1998) Prograde high- to ultrahigh-pressure metamorphism and exhumation of oceanic

DOI: https://doi.org/10.2138/am-2018-6460

sediments at Lago di Cignana, Zermatt-Saas Zone, western Alps. Lithos, 42, 147–189.

Scambelluri, M., and Rampone, E. (1999) Mg-metasomatism of oceanic gabbros and its control on Ti-clinohumite formation during eclogitization. Contributions to Mineralogy and Petrology, 135, 1–17.

Shen, T., Hermann, J., Zhang, L., Lü, Z., Padrón-Navarta, J.A., Xia, B., and Bader, T. (2015) UHP Metamorphism Documented in Ti-chondrodite- and Ti-clinohumite-bearing Serpentinized Ultramafic Rocks from Chinese Southwestern Tianshan. Journal of Petrology, 56, 1425–1458.

Smith, D. (1977) Titanochondrodite and titanoclinohumite derived from the upper mantle in the Buell Park kimberlite, Arizona, USA. A discussion. Contributions to Mineralogy and Petrology, 61, 213–215.

Spalla, M.I., Gosso, G., Marotta, A.M., Zucali, M., and Salvi, F. (2010) Analysis of natural tectonic systems coupled with numerical modelling of the polycyclic continental lithosphere of the Alps. International Geology Review, 52, 1268–1302.

Tiepolo, M., Bottazzi, P., Palenzona, M., and Vannucci, R. (2003) A laser probe coupled with ICP-double-focusing sector-field mass spectrometer for in situ analysis of geological samples and U-Pb dating of zircon. The Canadian Mineralogist, 41, 259–272.

Whitney, D.L., and Evans, B.W. (2010) Abbreviations for names of rock-forming minerals. American Mineralogist, 95, 185–187.

Zanoni, D., Rebay, G., Bernardoni, J., and Spalla, M.I. (2012) Using multiscale structural analysis to infer high-/ultrahigh-pressure assemblages in subducted rodingites of the Zermatt-Saas Zone at Valtournanche, Italy. Journal of the Virtual Explorer, 41, paper 6, 1-30.

Zanoni, D., Rebay, G., and Spalla, M.I. (2016) Ocean floor and subduction record in the Zermatt-Saas rodingites, Valtournanche, Western Alps. Journal of Metamorphic Geology, 34, 941-961.

FIGURE CAPTIONS

Figure 1 (a) Location of the studied area and simplified tectonic scheme of Western Alps. **(b)** Interpretative tectonic sketch of the upper Valtournanche; A – A': cross section trace in figure 1c. **(c)** Cross section (see Fig. 1b for location) on the western slope of Valtournanche (modified after Forster et al. 2004; Rebay et al. 2012). **(d)** Transposed Ti-Chn + Ti-Chu veins at low angle to S2. **(e)** Ol-rich layer folded by D2. **(f)** Ti-Chn porphyroclast mantled by Ti-Chu2 aggregate; crossed polars. **(g)** pre-D2 Cpx porphyroclast, with Ti-Chn + Ti-Chu exsolutions and Ti-Chn + Ti-Chu bearing fractures, wrapped by S2 foliation; crossed polars.

Figure 2. **(a)** M/Si vs. TiO_2 in Ti-Chu and Ti-Chn. **(b)** Pre-D2 P-T conditions (green and blue fields are for pre-D2 Ol porphyroclasts and pre-D2 to early D2 Ol polygonal aggregates, respectively). Reaction curves and stability fields of mineral assemblages are from Shen et al. (2015): in red curves from Ti-richer systems.

TABLES

Table 1. Selected Ti-Chu, Ti-Chn and Ol analyses.

DOI: https://doi.org/10.2138/am-2018-6460

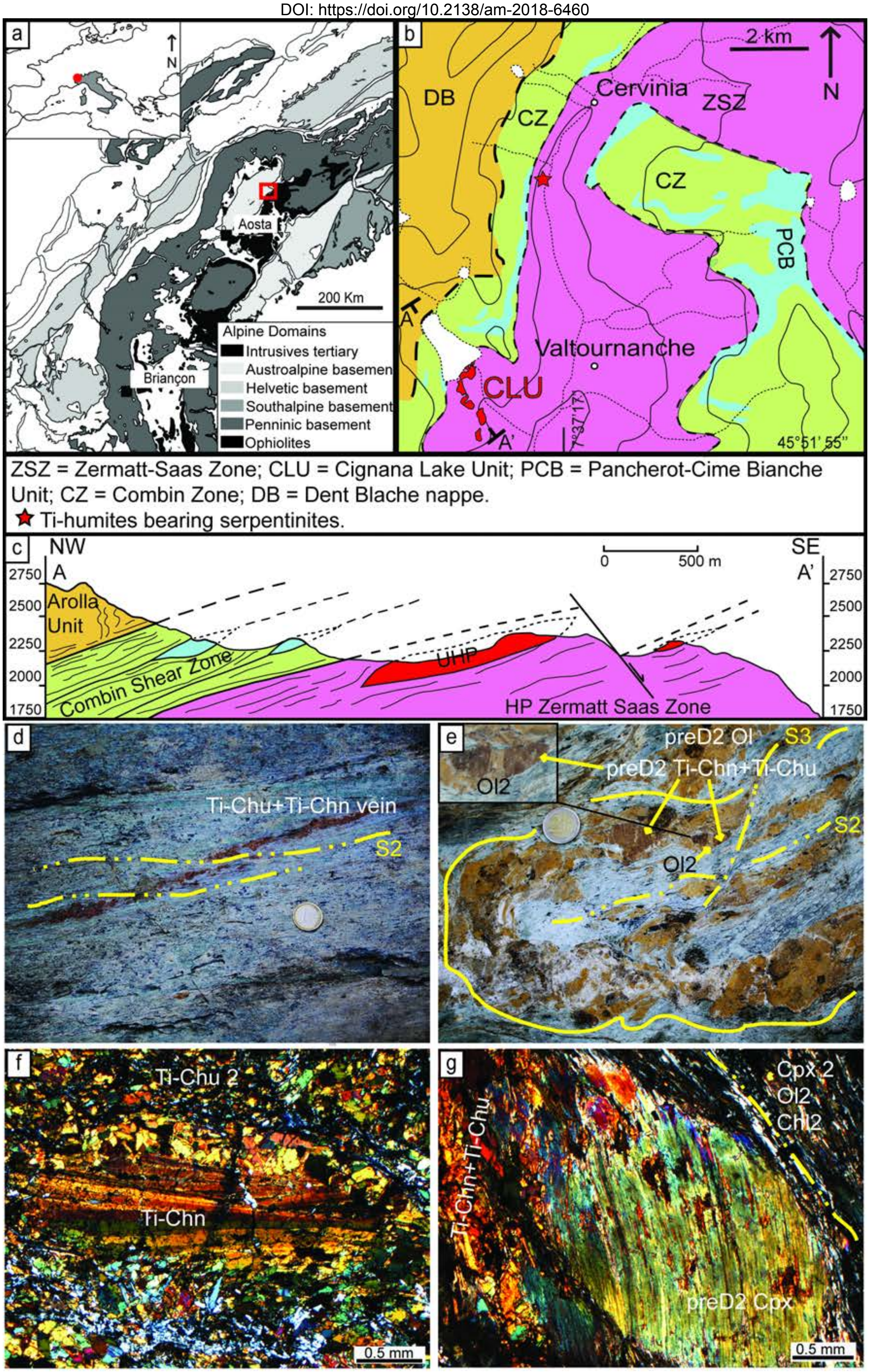

Figure 1
Revision 2

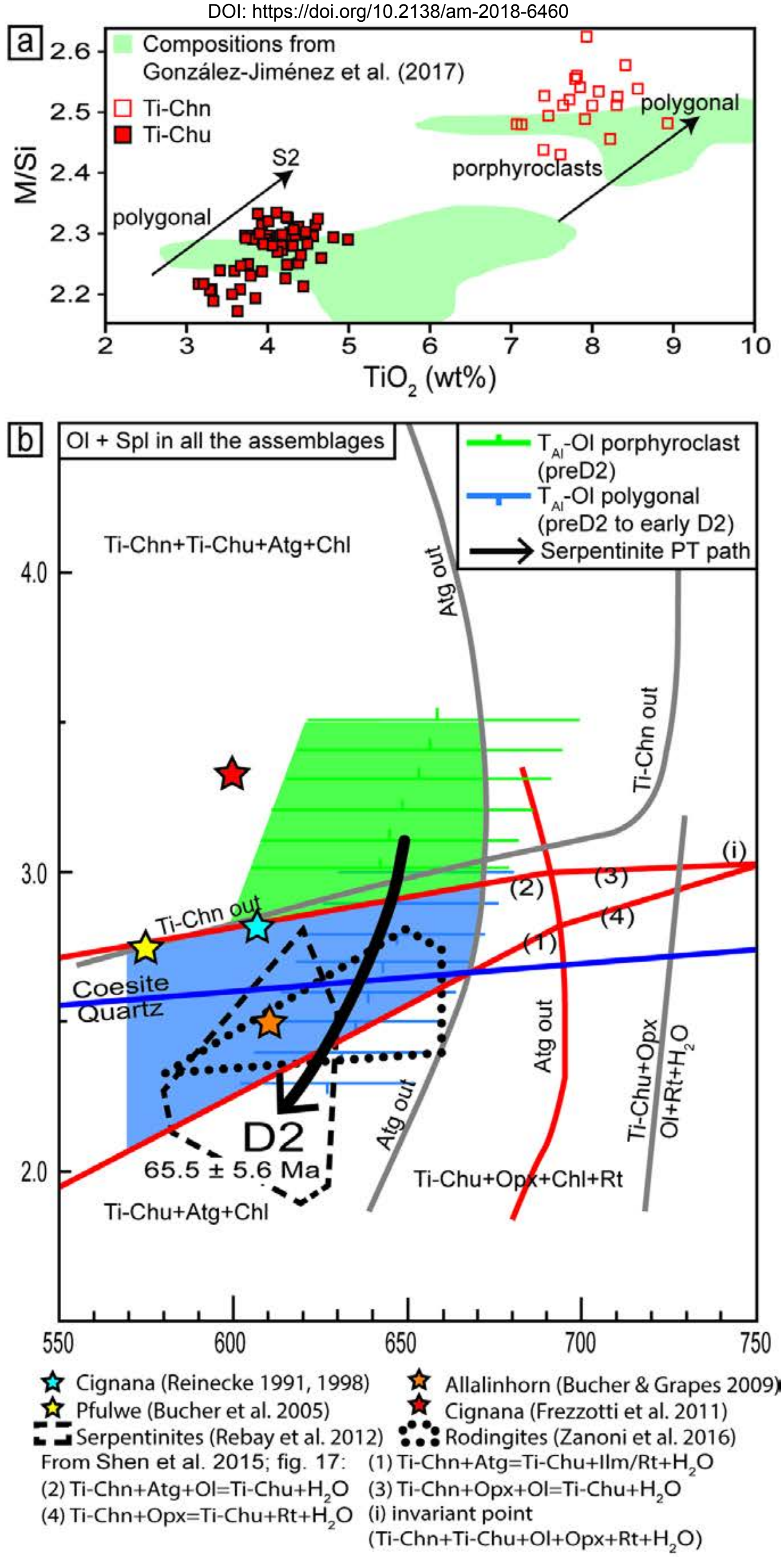

Figure 2

Revision2

DOI: https://doi.org/10.2138/am-2018-6460

	Ti-clinohumite		
Texture	in Ol	polygonal	S2
SiO_2	37.13	36.14	37.39
TiO_2	3.43	4.41	3.59
FeO	5.71	7.15	5.44
MnO	0.44	0.58	0.44
MgO	50.47	48.26	50.95
Sum	97.40	96.63	97.94
Si	4.01	3.98	4.01
Ti	0.28	0.37	0.29
Fe^{2+}	0.52	0.66	0.49
Mn	0.04	0.05	0.04
Mg	8.13	7.93	8.16
Cation sum	13.00	13.00	13.00

	Ti-chondrodite	
Texture	porphyroclast	polygonal
SiO_2	32.51	33.38
TiO_2	7.79	8.47
FeO	10.85	8.40
MnO	0.49	0.58
MgO	45.38	46.77
Sum	97.06	97.83
Si	1.97	1.99
Ti	0.35	0.38
Fe^{2+}	0.55	0.42
Mn	0.03	0.03
Mg	4.10	4.16
Cation sum	7.00	7.00

	Olivine	
Texture	porphyroclast	polygonal
SiO_2	41.11	40.89
TiO_2	-	-
Al_2O_3	-	-
Cr_2O_3	-	-
FeO	8.20	8.80
MnO	0.35	0.33
MgO	50.17	49.76
NiO	0.11	0.13
Sum	99.94	99.99
Si	1.00	1.00
Ti	-	-
Fe^{2+}	0.17	0.18
Mn	0.01	0.01
Mg	1.82	1.81
Ni	0.00	0.00
Cation sum	3.00	3.00
Al (ppm)	0.42	1.47
Cr (ppm)	7.67	2.11

Revision 2